LAWRENCE
LIVERMORE
NATIONAL
LABORATORY

LLNL-JRNL-804159

Radiation damage and annealing of three coaxial n-type germanium detectors: Preparation for spaceflight missions to asteroid 16 Psyche and Mar's moon Phobos

M. Burks

February 3, 2020

Nuclear Instruments and Methods in Physics, A

Disclaimer

Nuclear Inst. and Methods in Physics Research, A 942 (2019) 162409

Contents lists available at ScienceDirect

Nuclear Inst. and Methods in Physics Research, A

journal homepage: www.elsevier.com/locate/nima

Radiation damage and annealing of three coaxial n-type germanium detectors: Preparation for spaceflight missions to asteroid 16 Psyche and Mars' moon Phobos

Patrick N. Peplowski [a,*], Morgan Burks [b], John O. Goldsten [a], Samuel Fix [a], Lena E. Heffern [b,1], David J. Lawrence [a], Zachary W. Yokley [a]

[a] Johns Hopkins Applied Physics Laboratory, 11100 Johns Hopkins Road, Laurel MD 20723, USA
[b] Lawrence Livermore National Laboratory, 7000 East Avenue, Livermore CA 94550, USA

ARTICLE INFO

Keywords:
High-purity germanium
Cosmic rays
Radiation damage
Planetary nuclear spectroscopy

ABSTRACT

Three n-type high-purity germanium (HPGe) detectors were irradiated with protons at solar and galactic cosmic ray energies, with fluences corresponding to ≥3 years of exposure to the interplanetary radiation environment. Following 1 GeV proton irradiations (8×10^8 protons cm^{-2}), annealing of the detectors at 105° and 115 °C resulted in full energy resolution recovery after 240 and 140 h of annealing, respectively. A second irradiation, consisting of 7.25×10^9 protons cm^{-2} with a solar-proton-like energy spectrum, resulted in full recovery within <316 h of annealing at 105 °C. Prior spaceflight experience raised concerns about annealing-induced leakage currents. During this study, one of the three detectors was annealed for a cumulative time of 57 days, and there was no evidence for increased leakage currents. However, gamma-ray photopeak detection efficiency was found to be strongly anti-correlated with cumulative anneal time for all three detectors. The energy- and time-dependence of the efficiency loss is consistent with the loss of active volume at the inner borehole, which we attribute to thermal diffusion of the lithium contact during annealing. The data collected during this study validate aspects of the design of two in-development planetary gamma-ray spectrometers; one to the asteroid (16) Psyche and one to Mars' moon Phobos. The annealing strategy and operations concepts for these two instruments are informed by the results of this study.

1. Introduction

High-purity germanium (HPGe) gamma-ray spectrometers (GRS) play a vital role in space-science research, including astrophysics, solar physics, and planetary science missions. HPGe typically provides full-width at half-maximum (FWHM) energy resolution values of ~0.2% @ 1332 keV, the state-of-the-art performance. This leads to improved gamma-ray peak identification capabilities and superior signal-to-background as compared to competing technologies. Preserving the energy resolution performance of HPGe following exposure to the space radiation environment requires in-flight annealing (heating) of the HPGe crystal to remove radiation-induced lattice defects that act as charge traps. The frequency, duration, and maximum anneal temperature needed for full performance recovery depend on the characteristics (fluence, energy spectrum, and particle species) of the damage-inducing radiation.

For planetary science missions, radiation damage is accrued during the cruise through interplanetary space and during prime science operations at the target object of interest. The radiation of concern is the large flux ($\geq10^8$ cm^{-2} yr^{-1}) of high-energy (10 to >10,000 MeV) protons, both solar and galactic in origin. The radiation damage induced by these protons produces disordered regions in the HPGe crystal that act as charge collection traps (e.g. [1]). Charge trapping results in incomplete charge collection, which manifests as low-energy tailing on gamma-ray photopeaks. The HPGe-based GRS systems on the Mars Odyssey [2], Mercury MESSENGER [3], and lunar SELENE/Kaguya [4] missions all experienced degraded energy resolution as a result of this type of radiation damage.

Radiation damage to HPGe crystals can be repaired in-flight by annealing the HPGe crystal. Annealing restores the nominal HPGe lattice structure, removing charge trapping sites and thus restoring the performance of the GRS. Annealing operations for the Mars Odyssey, SELENE/Kaguya, and MESSENGER GRS systems resulted in incomplete energy resolution recovery (e.g. [5–7]) due to infrequent annealing at low (≤85 °C) temperatures. Laboratory testing has shown that 85 °C is

* Corresponding author.
E-mail address: Patrick.Peplowski@jhuapl.edu (P.N. Peplowski).
[1] Current affiliation: School of Earth and Space Exploration, Arizona State University, Tempe AZ, 85287, USA.

https://doi.org/10.1016/j.nima.2019.162409
Received 14 May 2019; Received in revised form 11 July 2019; Accepted 17 July 2019
Available online 19 July 2019

insufficient for full recovery of damage resulting from cosmic-ray (CR) like protons, regardless of the anneal duration [8–13].

The astrophysics mission INTEGRAL, which has 19 HPGe detectors, routinely achieves full energy-resolution recovery following its semi-annual, ~40-hr-long annealing operations at 105 °C [14]. As of 2017, 27 annealing operations had been performed for INTRGRAL over 13.5 years, and the initial energy resolution of the system (3.0 keV @ 1778 keV) has generally been maintained [13]. The INTEGRAL spacecraft is within the Earth's magnetosphere and experiences a different radiation environment than an interplanetary mission, however both INTEGRAL and MESSENGER energy resolution (FWHM) degraded at nominal rate of ~0.005 to 0.01 keV/day. Thus, the INTEGRAL experience is evidence that higher-temperature annealing of planetary science GRS systems will also provide full energy resolution recovery.

Flight experience with the MESSENGER GRS revealed periodic increases in leakage current that were correlated with annealing operations (Appendix). Leakage currents result from the introduction of small electrical pathways between the high-voltage contact on the HPGe crystal, introducing noise into the signal chain that manifests as peak broadening and thus degraded energy resolution. We attributed MESSENGER's leakage current problem to the introduction of outgassed surface contaminants on the HPGe surface, released during routine annealing operations [7]. The sealed encapsulation of the MESSENGER GRS HPGe crystal trapped the contaminants in the vicinity of the HPGe, where some settled on the exposed (non-passivated) surface of the crystal.

Annealing can also lead to thermal diffusion of the high-voltage contact on the crystal, reducing the active volume of HPGe and leading to a loss of gamma-ray detection efficiency. Ground-based annealing of n-type detectors has shown that this can be a significant issue; *Owens et al.* [15] observed a 17% loss of gamma-ray detection efficiency in n-type HPGe following 100 days of annealing at 100 °C. There is some evidence for <10% efficiency loss in the MESSENGER GRS (Appendix), however that result is inconclusive and efficiency loss is expected to be reduced at the lower annealing temperatures (85 °C) of the MESSENGER GRS. Annealing-induced efficiency loss needs to be quantified for future planetary GRS investigations.

The MESSENGER GRS engineering team is developing two HPGe-based GRS systems for launch in the early 2020's. The first is for the Psyche mission to asteroid (16) Psyche (Psyche Gamma-Ray and Neutron Spectrometer, GRNS; [16]). Psyche is set to launch in 2022 and arrive at (16) Psyche in 2026, following a 3.5-year-long cruise through interplanetary space. The second GRS is for the Martian Moon eXploration (MMX) mission to Mars' largest and innermost moon, Phobos. That instrument is called Mars-moon Exploration with GAmma-rays and Neutrons (MEGANE; [17]). MMX is set to launch in 2024 and arrive in the Mars system in 2026. A major goal of the Psyche GRNS and MEGANE engineering development efforts is to preserve the pre-launch energy resolution of those systems throughout cruise and prime science operations, while limiting increases in leakage current and efficiency loss associated with annealing. These goals require modifications relative to the heritage MESSENGER GRS design.

We designed a new GRS sensor for planetary science applications – GeMini Plus – based on the MESSENGER GRS design, but with modifications designed to addresses lessons learned from MESSENGER GRS flight experience [18,19]). GeMini Plus serves as the core of the Psyche GRNS and MEGANE instruments. GeMini Plus has the capability to anneal at temperatures up to 115 °C, which should allow full energy resolution recovery per INTEGRAL in-flight experience. GeMini Plus also incorporates a vented HPGe encapsulation to avoid annealing-induced build-up of contaminants, and a passivated detector to prevent any remaining contaminants from inducing leakage currents.

We report the results of an experimental campaign to irradiate and anneal three GeMini Plus units. The goal of this effort was to demonstrate full performance recovery following exposure to a space-radiation-like proton environment and subsequent annealing. Unlike prior irradiation and annealing studies, this effort incorporated realistic CR proton energy spectra and irradiation of warm detectors — a important distinction given that the Psyche GRNS and MEGANE instruments will not be kept at cryogenic temperatures during their interplanetary cruise phases. The performance of the GeMini Plus systems was tracked as a function of irradiation dose and the annealing history. The results of this study directly inform ongoing planning for Psyche GRNS and MEGANE instrument operations.

2. Performance degradation in the space radiation environment

2.1. Overview

Protons with energies above ~50 MeV penetrate the housing and structural materials of a GRS instrument and reach the HPGe crystal. These particles can directly interact with Ge atoms, displacing them from their normal position in the crystal lattice and placing them in an interstitial position. Displacement of a single atom creates a Frenkel defect which, along with the displaced Ge atom, creates a charge-trapping site for normal charge carriers [20].

The energy required to displace a Ge atom from the crystal lattice is just 30 eV [21], thus a single CR proton can dislocate many Ge atoms along its path through the HPGe crystal. Secondary particles, both recoiling Ge atoms and spallation products, can dislocate additional Ge atoms in the HPGe crystal, propagating the damage and creating localized clusters of defects (disordered regions) that are ~10 nm across [21]. These disordered regions are efficient charge traps, and they dominate charge collection losses within the crystal [1].

In an undamaged HPGe crystal, gamma rays that deposit all of their energy in the HPGe appear as narrow, Gaussian-shaped peaks (called photopeaks) in the GRS pulse height spectrum. In heavily radiation damaged HPGe crystals, photopeaks develop low-energy tails whose magnitude is proportional to the amount of damage the HPGe crystal has received. Events in the tail are the events for which charge collection was incomplete and thus the event registers with a pulse height of lower magnitude than the photopeak. Peaks in a radiation-damaged HPGe system can be fit with an exponentially-modified Gaussian (EMG) function, which adds an exponential tail at low energies to the Gaussian peak (e.g. Supplemental Online Material of [22]). A common metric to characterize the accumulated radiation to an HPGe crystal is to track the ratio of the full-width at tenth maximum (FWTM) to the full-width at half maximum (FWHM). The FWHM is related to the width of the Gaussian portion of the peak, whereas the FWTM is dominated by the magnitude of the low-energy peak tailing. An undamaged detector has a FWTM/FWHM of 1.823 [20].

Reverse-diode (n-type) HPGe detectors are more resistant to radiation damage than the more common p-type HPGe. P-type HPGe shows significant energy resolution degradation after proton fluences of 1×10^7 protons cm^{-2}, whereas n-type HPGe requires $\geq5\times10^7$ protons cm^{-2} before significant damage is observed [23]. Additionally, n-type HPGe experiences less resolution degradation at increasing HPGe temperature during irradiation, and completely anneals following shorter anneals at lower temperatures [24]. This makes n-type HPGe the material of choice for spaceflight applications. The WIND, Mars Odyssey, INTEGRAL, SELENE, and MESSENGER spacecraft payloads all included n-type HPGe-based GRS systems.

In addition to protons, the space environment contains neutrons, alpha particles, and heavy (Z>2) ions. Neutrons produced via CR-spallation of spacecraft materials are common in the space radiation environment around a spacecraft. Laboratory tests have shown that it takes an order of magnitude more neutrons than protons to produce an equivalent degradation in energy resolution [25]. Thus, neutrons are generally of lesser concern than CR protons. CR alpha particles and heavy ions (Z>2) are both less abundant than CR protons (e.g. [26]) and less likely to penetrate HPGe-surrounding housing and structural material, making them an insignificant contributor to accumulated radiation damage in spaceflight HPGe systems. As a consequence, this and prior studies have focused on the effects of energetic protons in HPGe.

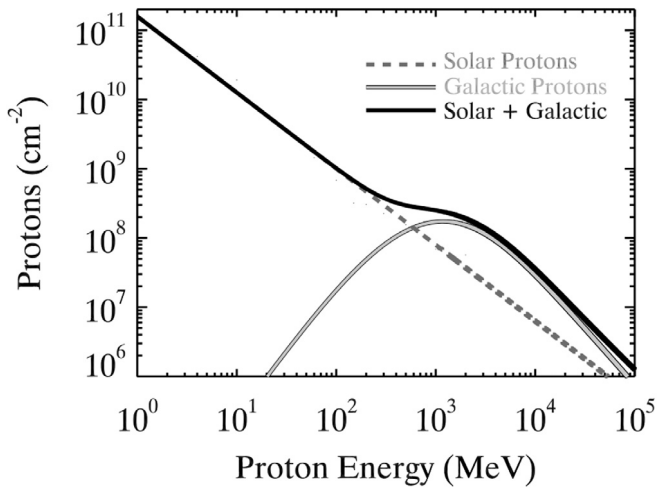

Fig. 1. A representative view of the cosmic-ray proton environment in interplanetary space, as relevant to the radiation exposure of a spaceflight HPGe-based gamma-ray spectrometer. The solar proton curve is the modeled cumulative environment for the Psyche spacecraft during its 3.5-year-long journey from Earth (1 AU) to the asteroid (16) Psyche (~3 AU). The galactic proton curve is the environment during typical solar conditions (solar modulation = 550 MV), calculated following the formalism of [30] and [31]. Additional details can be found in [32].

2.2. Space-radiation environment

Interplanetary space is filled with solar- and galactic-originating particles, called cosmic rays (CRs). Galactic cosmic rays (GCRs) consist of protons (~90%–95% by number), alpha particles (~5%–10%), heavy (Z>2) ions (<1%), and electrons (<1%), having energies up to >100 GeV per nucleon (Figure 1; e.g., [27]). The spectral shape and intensity of GCRs within the heliosphere varies in response to the 11-year-periodicity solar magnetic field. Energy-integrated (>30 MeV) GCR proton fluxes range from ~1.5 to 4.5 protons cm^{-2} s^{-1}.

Solar protons are also common in interplanetary space. Fig. 1 details a predicted differential energy spectrum for solar CR protons. The prediction is constructed from the statistical model of [28], which is based on historical solar-proton event data. This model was used to predict the frequency and intensity of events during the 3.5-year-long Psyche mission interplanetary cruise (August 2022 to January 2026) from 1 to 3.5 AU. The individual events were summed and divided by the cruise length to derive an effective "steady-state" environment, which is shown in Fig. 1. In reality, solar-originating protons arrive during distinct, randomly timed solar-proton events (SPEs) of varying intensity typically lasting hours to days.

During prime science operations, the dominant risk to HPGe energy resolution comes from SPEs. SPEs can deliver high fluences (10^7 to $>10^9$ cm^{-2}) of protons in a short time (typically a few days or less). *Pirard et al.* [29] studied the radiation damage produced by 50 to 60 MeV protons, typical proton energies for an SPE, and found asymmetric damage to crystals that resulted in a permanent loss of gamma-ray detection efficiency that is proportional to the HPGe volume that was damaged during irradiation. SPEs often result in spacecraft safing events, during which time power can be cut off from the payload. For a mechanically-cooled HPGe system, the consequence is an unplanned warming up cycle and removal of HV bias. As noted by [21], warmup of a radiation damaged crystal dramatically degrades energy resolution as the charge trap sites are filled. A warmed, radiation-damaged HPGe system typically requires an annealing cycle in order to return to pre-SPE energy resolution. Because measurement time in a GRS-favorable orbit is often limited, quick recovery from such an event is often crucial for meeting measurement objectives.

3. Experiment details

3.1. Sensors

The irradiation and annealing experiments described here used the GeMini-Plus HPGe gamma-ray sensors [18], developed under NASA's Maturation of Instrumentation for Solar System Exploration (MatISSE) program. The GeMini-Plus project had a stated goal of developing a low-resource GRS system whose performance is not limited by the radiation damage and leakage current problems experienced by the MESSENGER GRS flight system (see Appendix, and [7]). This experiment used three near-identical GeMini-Plus systems. For convenience, the units were named Tesla (Unit #1), Edison (Unit #2), and Westinghouse (Unit #3). Important characteristics for each HPGe crystal are detailed in Table 1.

The GeMini-Plus HPGe crystals adopted the MESSENGER-GRS-heritage design. They were 5-cm-length by 5-cm-diameter, closed-end coaxial crystals made from n-type HPGe. The HPGe crystals were provided by Canberra (now Mirion, Inc.), a change from the MESSENGER-heritage crystal manufacturer Ortec. Note that the length of the Westinghouse detector (~45 mm; Table 1) is shorter than Tesla and Edison (~51 mm), as the open end of Westinghouse required re-machining early in development to remove a damaged portion of the crystal.

Additional changes relative to the MESSENGER GRS include the inclusion of a passivated groove on the open end of the HPGe crystal to separate the high- and low-voltage contacts, and a vent-to-space design for the HPGe encapsulation to ensure a clean vacuum enclosure for the HPGe crystal. In contrast, MESSENGER had a WIND/TGRS-heritage [33] sealed encapsulation filled with 2 atm of dry N_2 that is thought to have contributed to the leakage current problem (Section 1). The vent-to-space design of GeMini-Plus mitigates this issue. For laboratory testing, vacuum was achieved via a pump-out port connected to a turbopump, which provided 10^{-6} Torr vacuum during all operations, including detector annealing.

GeMini-Plus has a flexible design that accommodates many different types of cryocoolers. For these experiments, we used a Sunpower CryoTel DS 1.5 Stirling cryocooler to achieve the nominal HPGe operating temperature of 90 K. The cryocooler was operated with a commercial power supply in closed-loop temperature regulation mode. A single Zener diode attached to the HPGe encapsulation is used for annealing. A temperature of 115 °C can be achieved from room temperature in approximately 10 h when providing 1 W to the Zener diode. Temperature sensors are located on the cryocooler cold finger and the HPGe encapsulation to monitor the system during cooling, annealing, and operation. Annealing operations are also performed in closed-loop temperature regulation. Throughout this manuscript, reported annealing times are the time that the encapsulation, and by extension the HPGe crystal, was held at the target temperature. Temperature ramp-up and ramp-down times were not included. Additional details on the design of the GeMini Plus systems can be found in [18,19].

3.2. Laboratory characterization

GeMini-Plus performance was characterized using an Ortec DSpec Pro multichannel analyzer. The DSpec provided the crystal bias voltage and performed all signal processing. The DSpec low-frequency reject option was enabled, and auto-pole zero was used at the beginning of each measurement set. Nominal operating parameters were −3000 V bias, and 8 μs rise-time with a 0.8 flat top, however these settings were varied during detector characterization tests of the depletion voltage and resolution versus shaping time, which were repeatedly characterized for each detector. As the temperature sensors introduced some noise into the signal processes chain, we unplugged the sensors during characterization tests. Before and after temperature measurements show that the HPGe crystal temperature was 90 K (±2 K) for all measurements.

Table 1
HPGe detector characteristic summary table.

Characteristic	N1 (Tesla)	N2 (Edison)	N3 (Westinghouse)[a]
Length (mm)[b]	50.8	50.7	~45
Diameter (mm)[b]	51.0	50.7	50.9
Borehole length (mm)[b]	38.0		~33
Borehole diameter (mm)[b]	8.0		
Depletion voltage (−V)	2500	2000	2000
Leakage current (pA)	<10	5	9.3
FWHM @ 1332 keV	2.18 ± 0.02	2.29 ± 0.02	2.21 ± 0.02
FWTM @ 1332 keV	4.03 ± 0.03	4.23 ± 0.03	4.07 ± 0.03
Relative efficiency@ 1332 keV[b]	24.9%	24.3%	–
Inner (n^+) Contact	Lithium (thermally diffused)		
Outer (p^+) Contact	Boron (ion implantation)		
Non-contacts (groove)	Passivated (proprietary material)		

[a]Westinghouse was re-machined from its original size (identical to Tesla and Edison) to a smaller length to remove a mechanical defect in the crystal on the open end prior to all testing described here.

[b]Per Canberra datasheet for as-delivered detector, in the standard efficiency geometry (25 cm from detector, quoted relative to a 3 cm × 3 cm NaI detector). This is not the efficiency of the crystal mounted in the GeMini cryostat. No efficiency measurement was made for the Westinghouse detector following re-machining.

Our experiments characterized energy resolution and relative photopeak detection efficiency over a wide range of energies (277–2615 keV) via the use of NIST-traceable gamma-ray sources, including ^{60}Co (1173, 1332 keV), ^{54}Mn (843 keV), ^{137}Cs (661 keV), and ^{228}Th (277, 584, 783, and 2615 keV). Here we restrict ourselves to reporting the performance at 1332 keV, an industry standard (ANSI N42) for characterizing GRS energy resolution. Sources were held in a measurement jig that ensured a fixed, repeatable source-to-detector-center distance of 15 (±0.2) cm for all measurements. This distance is perpendicular to the crystal length (bore hole axis). Vertically, the sources are fixed at the center of the crystal.

GeMini performance was characterized multiple times during each experiment. First, a pre-irradiation characterization measurement set was taken to provide the performance baseline. Next, a measurement set was acquired following the detector irradiation. Finally, a measurement set was acquired following each HPGe annealing operation. Each characterization included the following set of measurements:

1. Resolution at 1332 keV, with varying shaping times, using the ^{60}Co source,
2. Resolution and photopeak efficiency versus energy, at fixed shaping time of 8 μs, using the ^{60}Co, ^{54}Mn, ^{137}Cs, and ^{228}Th sources,
3. Resolution at 1332 keV versus bias voltage on the crystal, which provides a means of characterizing the depletion voltage (the minimum voltage at which the field is uniform throughout the crystal).

Measurements were run long enough to collect >10,000 events in the photopeaks of interest. Depletion voltage was determined as the lowest voltage at which the 1332-keV count rate reaches a plateau, which is evidence for a near-uniform electric field throughout the crystal volume. Many of the detector measurement sets also included a leakage current measurement, made possible because the preamplifier is DC-coupled to the low-voltage lithium contact. The leakage current was determined by reading the DC voltage offset of the preamplifier output, which is directly proportional to the leakage current (1 mV offset = 1 pA leakage current).

For each measurement, the peak rate and energy resolution of the gamma-ray photopeaks were determined from spectral fitting. An exponentially modified Gaussian (EMG) function was used, which fits both pristine photopeaks and peaks with low-energy tails resulting from radiation damage. For undamaged detectors, the tailing parameter is zero and the function becomes a standard Gaussian. Use of the EMG function for gamma-ray spectral fitting is discussed in the supplemental material of [22]. A numerical routine was developed to calculate FWHM and FWTM values from the EMG-fitted peak shape. Errors for the numerically-derived FWHM and FWTM values were propagated from the EMG fit parameter errors.

3.3. Proton irradiation experiments

3.3.1. Overview

Our GeMini detectors were irradiated at the NASA Space Radiation Laboratory (NSRL; [34]), located at the Brookhaven National Laboratory (BNL). The proton beam was provided by two 15-MV Tandem Van de Graaff accelerators, and further accelerated to our desired energy in the BNL Alternating Gradient Synchrotron booster. Beam bunches, which had a time width of 300-400 ms, were pulled from the booster every 3.5 s and directed toward the NSRL beamline, where a series of quadrupole magnets shaped the beam to a 20 cm × 20 cm square [35] that uniformly irradiated the detectors. The shaped beam bunches entered the open-air NSRL target room, where they traveled ~6 m to the target table.

The detectors were positioned on the target table, one at a time, on low-density polyethene foam blocks that were sized to keep the entire detector, but not the target table, in the path of the proton beam. This ensured that only primary, full-energy protons irradiated the detectors. The detectors were also encased in the polyethene foam to keep them in a fixed, upright position in the beamline during irradiation. The foam was chosen due to its low density and low nuclear charge (Z), which ensured minimal attenuation and downscattering of the protons.

The proton fluence on the detectors was monitored with an upstream ion chamber (IC). Prior to irradiation, the IC was calibrated against a NIST-traceable thimble ion chamber, and a detailed analysis has shown that the overall dose uncertainty of the NSRL system is 3.6% [36]. Once the target fluence for each irradiation was reached (see Sections 3.3.2 and 3.3.3), the irradiation run was automatically terminated. A downstream digital beam imager (DBI) provided horizontal and vertical profiles of the beam, which were used to confirm complete and uniform irradiation of the detectors in real time. This technique routinely achieves uniform irradiation, with <3% variance across the sample, for all particle species and energies [36].

Mechanically-cooled HPGe GRS systems are typically not cooled during interplanetary cruise to preserve power and cooler lifetime. This motivated our decision to perform the irradiation experiments with the detectors at room temperature, close to the temperature during interplanetary cruise. Irradiation of warm detectors differs from the majority of prior irradiation experiments, which irradiated detectors held at cryogenic temperature [8–11,23,25]. *Bruckner et al.* [9] noted that, in the 90–120 K range, energy resolution degradation scales with the detector temperature during irradiation. Thus, the prior studies noted above likely underestimate the accumulated radiation damage experienced by warm detectors in interplanetary space. This observation was a significant motivation for conducting the experiments detailed here.

Table 2
Proton irradiation energy spectrum details. For the second irradiation, mono-energetic beams were run sequentially, from 30 MeV to 2 GeV, to cover the entire energy range of interest.

Energy (MeV)	Proton flux (cm^{-2})	
	1st irradiation	2nd irradiation
30	–	3.99×10^9
60	–	1.45×10^9
100	–	6.80×10^8
150	–	3.18×10^8
200	–	3.04×10^8
300	–	2.26×10^8
500	–	1.56×10^8
1000	8×10^8	6.92×10^7
2000	–	5.68×10^7
Total	$\mathbf{8 \times 10^8}$	$\mathbf{7.25 \times 10^9}$

3.3.2. Irradiation #1

For the first irradiation experiment, all three detectors were irradiated with $8{\times}10^8$ protons cm^{-2}. This is the approximate number of ≥10 MeV GCR protons expected during an ~8-year-long interplanetary cruise. This number does not include contributions from solar CRs. A beam energy of 1 GeV was chosen for the first irradiation for several reasons, including:

1. 1 GeV is near the mean energy of GCR protons (Fig. 1),
2. 1 GeV protons are minimum ionizing particles (MIPs) in germanium, meaning that the amount of energy they deposit in the HPGe is representative of a wide range of proton energies (~500 to >10,000 MeV), and
3. This energy is similar to prior experiments that irradiated HPGe detectors with mono-energetic protons (1.5 GeV, [9,23]), facilitating comparison to other studies.

Our experiment uniformly illuminated the detectors from a single direction, which contrasts with uniform (4π) illumination expected for GCRs, however the fact that 1 GeV protons are MIPs means that even in the single-direction-irradiation, the entire HPGe volume was exposed to protons and subject to radiation damage. Performance of the GeMini detectors following irradiation #1 is discussed in Section 4.1.

3.3.3. Irradiation Experiment #2

Following the first irradiation experiment, the fully recovered Westinghouse detector was returned to NSRL for a second irradiation. This irradiation was performed using protons with energies from 30 MeV to 2 GeV. Per-energy fluences for each proton energy used in the irradiation are listed in Table 2. This energy environment is the predicted cumulative proton environment resulting from GCRs and predicted solar proton events occurring during Psyche's 3.5-year-long interplanetary cruise to asteroid (16) Psyche (Section 2.2 for details on the prediction). This irradiation had an integrated fluence of $7.3{\times}10^9$ protons cm^{-2}, similar to the experiment of *Owens et al.* [12], who irradiated HPGe sensors with solar-proton-like spectra of varying integrated fluences of $8{\times}10^8$, $6{\times}10^9$, and $6{\times}10^{10}$ protons cm^{-2}.

Proton beams with energies of 100 MeV and greater were provided to NSRL directly by the BNL Alternating Gradient Synchrotron. The 30 and 60 MeV beams were created from the 100 MeV beam through the use of energy degraders. Protons with energies <30 MeV were not included in this experiment, as they cannot penetrate the GeMini housing and thus do not interact with the HPGe crystal. Additionally, <30 MeV particles are sufficiently low in energy that they do not produce appreciable amounts of secondary particles that might otherwise reach the HPGe crystal.

For the second irradiation, the inclusion of low-energy particles raises the importance of including a realistic GRS sensor assembly. The MEGANE and the Psyche GRNS will include an anti-coincidence shield (ACS) to veto GCR signals from the HPGe measurements. GeMini does not include an ACS, so an ACS mass model, based on the Psyche GRNS mechanical design, was included in this irradiation. The ACS mass model was placed upstream of GeMini, and thus energy downscattering of protons in the ACS, prior to reaching the HPGe, is included in the experiment in a way that closely mimics that expected in flight for the MEGANE and Psyche GRNS.

As with irradiation #1, the experiment uniformly illuminated the detector from a single direction. In this scenario, the damage resulting from the lower-energy (<300 MeV) protons is concentrated in the upstream side of the HPGe crystal, similar to the irradiation of *Pirard et al.* [29]. Those authors modeled the physical distribution of damage sites for 50–60 MeV protons, showing that the damage was concentrated along the upstream side. We performed comparable modeling a found a similar damage distribution for the <300 MeV protons. Higher energies resulted in more uniform damage to the HPGe crystal.

4. Results: Proton irradiation

4.1. Energy resolution recovery – 1 GeV proton irradiation

4.1.1. Annealing at 105 °C

Following irradiation #1, the GeMini units were returned to the Johns Hopkins University Applied Physics Laboratory (APL) for post-irradiation characterization and annealing. Fig. 2 summarizes a subset of the results from these characterization and annealing studies. The figure clearly illustrates the manifestation of radiation damage — low-energy tailing on the gamma-ray peak (Section 2.1). The figure also highlights the restoration of the peak shape following many hours of annealing. Detector-by-detector results are detailed below.

The Edison detector was characterized first, including post-irradiation characterization followed by five annealing operations at 105 °C (Table 3). The post-irradiation FWTM/FWHM ratio for Edison was 3.1 ± 0.1, which is 1.7 times its pre-irradiation value of 1.85 ± 0.02. The energy resolution was fully recovered (returned to pre-irradiation resolution) sometime between the 4th and 5th annealing operations, which had cumulative anneal times of 186 and 378 h, respectively.

Next, the Tesla detector underwent post-irradiation characterization and a single 5-hr-long anneal at 105 °C. Like Edison, Tesla had a post-irradiation FWTM/FWHM ratio of 3.1 ± 0.1. The short (5 hr) anneal at

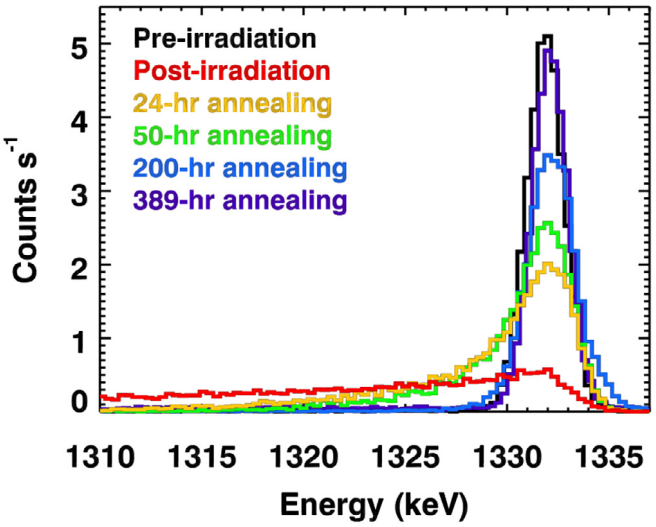

Fig. 2. A representative sample of 1332-keV photopeak measurements, acquired at different points during the experiment, with the Tesla detector. The data illustrate the Gaussian shape of a gamma-ray photopeak, the tailing induced by radiation damage, and the recovery following annealing operations. A color version of this figure can be found online.

Table 3
Detector activities - Edison.

Activity	Date[a] (mm/dd/yy)	Anneal		Depletion voltage (−V)	Performance at 1332 keV			
		Temperature, Duration	Cumulative time		FWHM (keV)	FWTM (keV)	FWTM/ FWHM	Efficiency[b]
Pre-irradiation	10/4/17	n/a	n/a	2000	2.29 ± 0.02	4.23 ± 0.03	1.85 ± 0.02	100 ± 1.2%
Irradiation[c]	10/16/17	n/a	n/a	n/a	n/a	n/a	n/a	n/a
Post-irradiation	10/30/17	n/a	n/a	–	28.2 ± 0.2	88.0 ± 1.4	3.1 ± 0.1	–
Post-Anneal #1	11/3/17	105 °C, 21 h	21 h	<1000	5.7 ± 0.2	14.9 ± 0.3	2.6 ± 0.1	98.9 ± 1.0%
Post-Anneal #2	11/6/17	105 °C, 21 h	42 h	<1000	4.3 ± 0.2	10.5 ± 0.2	2.5 ± 0.1	97.8 ± 1.2%
Post-Anneal #3	11/10/17	105 °C, 48 h	90 h	~1500	3.5 ± 0.1	8.3 ± 0.1	2.4 ± 0.1	98.0 ± 1.2%
Post-Anneal #4	11/16/17	105 °C, 4 days	186 h	~1500	2.7 ± 0.1	5.4 ± 0.1	2.0 ± 0.1	96.1 ± 1.2%
Post-Anneal #5	11/27/17	105 °C, 8 days	378 h	~1500	2.11 ± 0.02	3.90 ± 0.03	1.85 ± 0.02	95.8 ± 1.2%

[a]For annealing activities, date refers to the post-anneal performance measurements.
[b]Efficiency calculated relative to the pre-irradiation value.
[c]8×10^8 protons cm^{-2}; near the mean energy of GCR protons, and roughly equivalent to the total number.
n/a = not applicable, e.g. no anneal was performed.
"–" = data was insufficient to derive the value of interest.

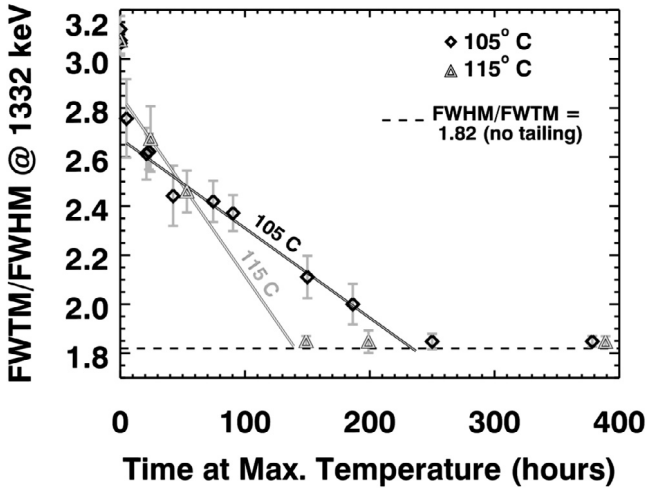

Fig. 3. Summary of the energy resolution recovery for all three GeMini detectors, following 1 GeV proton irradiation (irradiation #1). Data is divided by annealing temperature (see legend). 105° measurements were made using all three detectors, 115 °C measurements were made on the Tesla detector only. Linear fits to the post-annealing data, which excluded full-recovery data, provide estimated time to full recovery values of 240 and 140 h for the 105° and 115 °C annealing, respectively. These values are the intersection of the fits with the FWHM/FWTM = 1.82 line. All data values are listed in Tables 3–5.

105 °C was to test the hypothesis that HPGe radiation damage consists of "shallow" and "deep" traps, with the former being repaired quickly (hours of annealing) and the latter taking longer (days of annealing). The FWTM/FWHM ratio following the quick anneal was of 2.8 ± 0.2. All further anneals on Tesla were performed at a higher temperature of 115 °C and are discussed in Section 4.1.2.

Following the full set of Tesla annealing operations, the Westinghouse detector underwent post-irradiation characterization and four annealing operations at 105 °C (Table 4). Like Edison and Tesla, Westinghouse had a post-irradiation FWTM/FWHM ratio of 3.1 ± 0.1. The detector fully recovered (returned to pre-irradiation resolution) sometime between the 3rd and 4th annealing operations, which had cumulative anneal times of 150 and 250 h, respectively.

The FWTM/FWHM ratio for all 105 °C annealing operations are plotted as a function of cumulative anneal time in Fig. 3. We note that the Edison (Table 3) and Westinghouse (Table 4) data are completely consistent, suggesting that detector-to-detector variations are not a consideration. A linear fit to the post-irradiation, pre-full-recovery data indicates that full energy resolution recovery (FWTM/FWHM = pre-irradiation value) occurred following 240 h of annealing. Although no annealing operation on any detector ended with this cumulative anneal time, the third Westinghouse anneal was close (250 h) and its performance was consistent with full recovery (FWTM/FWHM = 1.85 ± 0.03).

4.1.2. Annealing at 115 °C

Anneal operations on Tesla were performed at 115 °C to test the hypothesis that higher annealing temperatures would result in shorter time needed for full energy resolution recovery, as indicated by prior studies [9,11]. Tesla annealing operations 2–6 were performed at 115 °C, reaching a cumulative anneal time at this temperature of 389 h (Table 5). Tesla experienced full energy resolution recovery between anneals #3 (53 h) and #4 (149 h). The FWTM/FWHM ratio following all 115 °C anneals are plotted as a function of cumulate anneal time in Fig. 3. A linear fit to the post-irradiation, pre-full-recovery data indicates that full energy resolution recovery (FWTM/FWHM = pre-irradiation value) occurred at approximately 140 h, close to the cumulative anneal time of annealing operation #4 (149 h).

4.2. The cosmic-ray proton spectrum irradiation

Following full energy resolution recovery after irradiation #1, the Westinghouse detector was returned to NSRL and exposed to the predicted Psyche cruise (solar + galactic) proton environment (see Table 2). Following irradiation and return to APL, the post-irradiation performance of Westinghouse was characterized, and three subsequent annealing operations at 105 °C were performed (anneals #5, #6, and #7; Table 4). The post-irradiation-#2 total anneal time was 316 h, and the cumulative anneal time on Westinghouse was then 566 h.

A noisy signal chain compromised three of the post-irradiation measurements of Westinghouse. As a consequence, no performance metrics are reported for those measurements (Table 4). The issue was repaired following anneal #7. Characterization of the performance following this anneal showed full recovery to Westinghouse's pre-irradiation performance (FWTM/FWHM = 1.85 ± 0.1). Due to the lack of quality measurements following anneals #5 and #6, we are restricted to concluding that the radiation damage resulting from the full Psyche cruise proton dose was fully repaired following <316 h of annealing at 105 °C.

4.3. Radiation damage and depletion voltage

We include the depletion voltage curves for Westinghouse as a function of irradiation and anneal event (Fig. 4). The curves highlight the fact that radiation damage changes the effective impurity level of the HPGe crystal, changing (lowering) the HV bias required to achieve uniform electric field across the crystal volume. Thus, depletion voltage is an independent indicator of radiation damage, and the fact that we observe a return to the original depletion voltage that coincides with full energy resolution recovery is evidence that the HPGe crystal has fully recovered from the irradiations following the annealing activities.

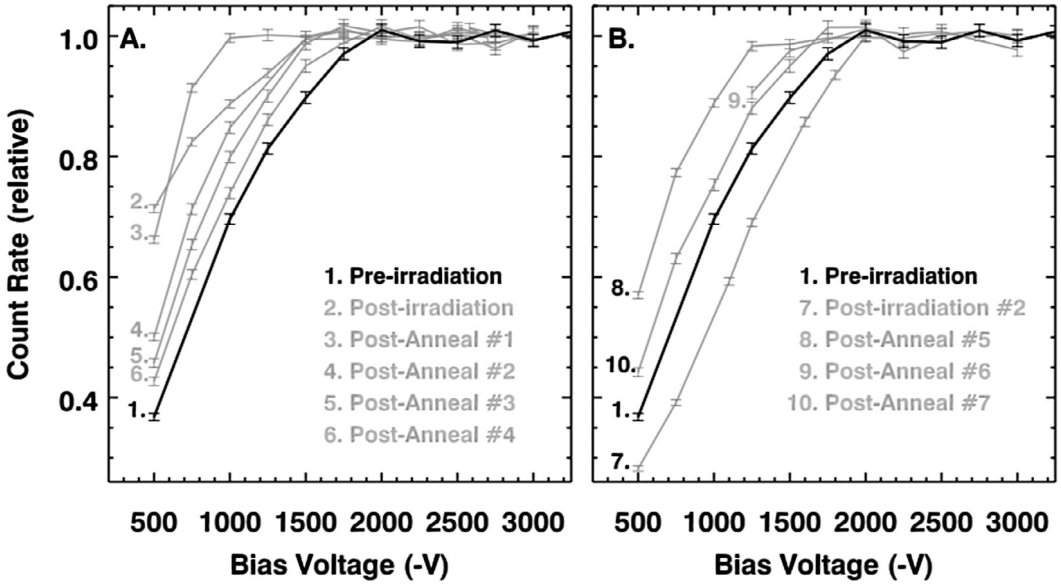

Fig. 4. Depletion curves for the Westinghouse detector, measured at various points during the irradiation experiment (see legend). Count rates are normalized to plateau at one to remove the effects of the annealing-induced efficiency loss (see Section 4.4).

Table 4
Detector activities - Westinghouse.

Activity	Date[a] (mm/dd/yy)	Anneal		Depletion voltage (−V)	Performance at 1332 keV			
		Temperature, Time	Cumulative time		FWHM (keV)	FWTM (keV)	FWTM/ FWHM	Efficiency[b]
Pre-irradiation	9/26/17	n/a	n/a	2000	2.21 ± 0.02	4.07 ± 0.03	1.84 ± 0.02	100 ± 1.4%
1st Irradiation[c]	10/16/17	n/a	n/a	n/a	n/a	n/a	n/a	n/a
Post-irradiation	4/11/18	n/a	n/a	1500	15.6 ± 0.2	47.8 ± 0.5	3.1 ± 0.1	–
Post-Anneal #1	4/16/18	105 °C, 23 h	23 h	1000	4.5 ± 0.1	11.8 ± 0.2	2.6 ± 0.1	98.3 ± 1.4%
Post-Anneal #2	4/20/18	105 °C, 52 h	75 h	<1500	3.1 ± 0.1	7.5 ± 0.1	2.4 ± 0.1	95.7 ± 1.2%
Post-Anneal #3	4/25/18	105 °C, 75 h	150 h	1500	2.7 ± 0.1	5.7 ± 0.1	2.1 ± 0.1	97.3 ± 1.4%
Post-Anneal #4	5/1/18	105 °C, 100 h	250 h	2000	2.17 ± 0.03	4.01 ± 0.04	1.85 ± 0.03	95.7 ± 1.4%
2nd Irradiation[d]	6/4/18	n/a	250 h	n/a	n/a	n/a	n/a	n/a
Post-irradiation	11/6/18	n/a	250 h	2000	–	–	–	–
Post-Anneal #5	11/12/18	105 °C, 102 h	352 h	1250	–	–	–	–
Post-Anneal #6	11/18/18	105 °C, 60 h	412 h	2000	–	–	–	–
Post-Anneal #7	11/28/18	105 °C, 154 h	566 h	2000	2.2 ± 0.1	4.0 ± 0.1	1.85 ± 0.1	93.4 ± 1.4%
Post-Anneal #8	2/01/19	105 °C, 569 h	1135 h	2000	2.1 ± 0.1	3.9 ± 0.1	1.85 ± 0.1	90.0 ± 1.1%
Post-Anneal #9	5/07/19	105 °C, 236 h	1371 h	2000	1.98 ± 0.04	3.65 ± 0.04	1.85 ± 0.04	90.7 ± 1.0%

[a]For annealing activities, date refers to the post-anneal performance measurements.
[b]Efficiency calculated relative to the pre-irradiation value.
[c]8×10^8 protons cm^{-2}; near the mean energy of GCR protons, and roughly equivalent to the total number of GCR protons incident on a surface over 8 years of exposure to GCRs.
[d]Mixed energy beam, see Table 2 for details.
n/a = not applicable, e.g. no anneal was performed.
"–" = data was insufficient to derive the value of interest.

Table 5
Detector Activities - Tesla.

Activity	Date[a] (mm/dd/yy)	Anneal		Depletion voltage (−V)	Performance at 1332 keV			
		Temperature, Time	Cumulative time[b]		FWHM (keV)	FWTM (keV)	FWTM/ FWHM	Efficiency[d]
Pre-irradiation	9/11/17	n/a	n/a	2500	2.18 ± 0.02	4.03 ± 0.03	1.85 ± 0.02	100 ± 1.2%
Irradiation[c]	10/16/17	n/a	n/a	n/a	n/a	n/a	n/a	n/a
Post-irradiation	2/22/18	n/a	n/a	<1500	18.4 ± 0.2	56.6 ± 0.8	3.1 ± 0.1	–
Post-Anneal #1	2/26/18	105 °C, 5 h	n/a	<1000	10.3 ± 0.5	28.4 ± 0.9	2.8 ± 0.2	97.5 ± 1.2%
Post-Anneal #2	3/1/18	115 °C, 24 h	24 h	1250	4.6 ± 0.2	12.3 ± 0.3	2.7 ± 0.1	97.5 ± 1.4%
Post-Anneal #3	3/6/18	115 °C, 29 h	53 h	1750	3.7 ± 0.1	9.1 ± 0.2	2.5 ± 0.1	97.3 ± 1.4%
Post-Anneal #4	3/12/18	115 °C, 95 h	149 h	1750	2.26 ± 0.02	4.18 ± 0.03	1.85 ± 0.03	97.3 ± 1.4%
Post-Anneal #5	3/19/18	115 °C, 50 h	199 h	1750	2.29 ± 0.05	4.23 ± 0.05	1.85 ± 0.05	96.4 ± 1.3%
Post-Anneal #6	3/30/18	115 °C, 190 h	389 h	1750	2.02 ± 0.02	3.73 ± 0.03	1.85 ± 0.03	93.7 ± 1.3%

[a]For annealing activities, date refers to the post-anneal performance measurements.
[b]Cumulative time at 115 ° C.
[c]8×10^8 protons cm^{-2}; near the mean energy of GCR protons, and roughly equivalent to the total number of GCR protons incident on a surface over 8 years of exposure to GCRs.
[d]Efficiency calculated relative to the pre-irradiation value.
n/a = not applicable, e.g. no anneal was performed.
"–" = data was insufficient to derive the value of interest. See Section 4.2 for details.

4.4. HPGE leakage current

Two final annealing operations (#8 and #9) were carried out on Westinghouse, following its full recovery from irradiation #2, for the purpose of characterizing the impact of annealing on detector leakage current. This study was motivated by MESSENGER GRS flight experience, as that instrument experienced a steady increase in leakage current as a function of cumulative anneal time (see Appendix). When MESSENGER GRS reached 40 days of cumulate annealing, predominantly at 85 °C, the leakage current was sufficiently high (1 nA) that it compromised the energy resolution of the GRS measurements.

The final Westinghouse anneals (#8 and #9) took the total cumulative anneal time on Westinghouse to 1371 h (57 days), well beyond the cumulative anneal time of the MESSENGER GRS. No increase in the leakage current, relative to the original (pre-annealing) value of <10 pA was observed for Westinghouse following the final anneal. This led us to conclude that the vented encapsulation and passivated surface of the GeMini-Plus design have resolved the MESSENGER leakage-current issue, which *Evans et al.* [7] attributed to the build-up of annealing-outgassed contaminants on the HPGe crystal.

4.5. Gamma-ray detection efficiency loss

The measured counting rate for the 1332-keV ^{60}Co gamma ray – calculated from the fitted peak area, divided by the detector livetime and corrected for the natural decay of the ^{60}Co source – decreased as a function of cumulative anneal time (Fig. 5) for all of our measurements. For our longest anneal times (>1000 h of cumulative annealing at 105 °C on Westinghouse), the gamma-ray detection efficiency was ~90% of its initial, pre-annealing value. Hypotheses for loss of gamma-ray detection efficiency in n-type HPGe sensors include formation of slightly-conducting surface layers leading to surface charging effects [37], loss of active volume due to thermal diffusion of the Li low-voltage contact located within the detector borehole (e.g. [15]), and formation of dead regions in heavily irradiated portions of the crystal [29].

Following anneal #8 (1135 h), the efficiency of Westinghouse was measured at ~20 different HPGe temperatures ranging between 67 K to 98 K. The lack of a temperature-dependent efficiency allowed us to rule out the surface charging phenomenon, which exhibits a strong temperature dependence [37]. We then used radiation transport modeling to test loss of active volume. The model was built using a custom application of Geant4, built from the AnaEx01 example but modified to incorporate standard Geant4 physics lists (Shielding) and the general particle source (GPS) primary particle generator. Additional details on these modifications are detailed in [32].

Two sets of models were run – the first decreased the volume of the HPGe crystal from the outside (outer B contact) inward, the second from the inside (inner Li contact) outward. Fig. 6 details the model HPGe geometry. Inactive volumes of the crystal were still composed of Ge, but were not part of the Geant4 volume in which gamma-ray events were tallied. Thus, scattering and attenuation losses in the dead volumes were preserved. Our model incorporated gamma-ray sources at the same position as the sources used for our laboratory measurements (Section 3.2), and a full material model of the GeMini units and HPGe crystal geometry. The gamma-ray photopeak detection efficiency values for the 661- and 1332-keV gamma rays were modeled and plotted as a function of the volume of the active area of the model HPGe crystal in Fig. 7 (right).

The measured 661- and 1332-keV photopeak efficiency, as a function of cumulative 105 °C anneal time, is shown in Fig. 7 (left). 661- and 1332-keV gamma rays are included because they have different mean free paths in Ge (2.6 and 3.8 cm, respectively). While both gamma rays sample the entire volume, the 1332-keV gamma ray more effectively samples the inner core of the HPGe crystal. Thus, the difference in the efficiency loss at these two gamma-ray energies is an indicator of the location of the inactive volume. This is supported by the model (Fig. 7, right), which predicts different behavior for the efficiency at these two energies, depending on the location of the inactive volume.

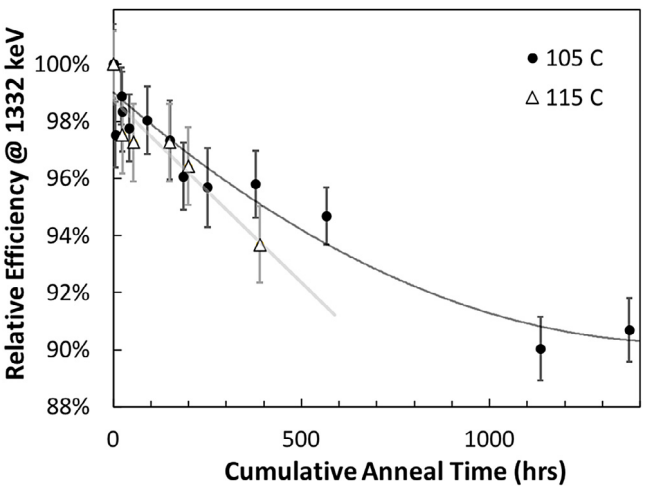

Fig. 5. Photopeak efficiency for detecting 1332-keV gamma rays from ^{60}Co, plotted as a function of the cumulative anneal time. Efficiency is relative to the pre-annealing value. Data are from all three GeMini detectors, and include annealing at 105 °C (solid black circles) and 115 °C (black outlined triangles). 105° measurements were made using all three detectors, 115 °C measurements were made on the Tesla detector only. Linear fits to the data are performed separately for the 105 °C (black line) and 115 °C (gray line) data. Data values are listed in Tables 3–5.

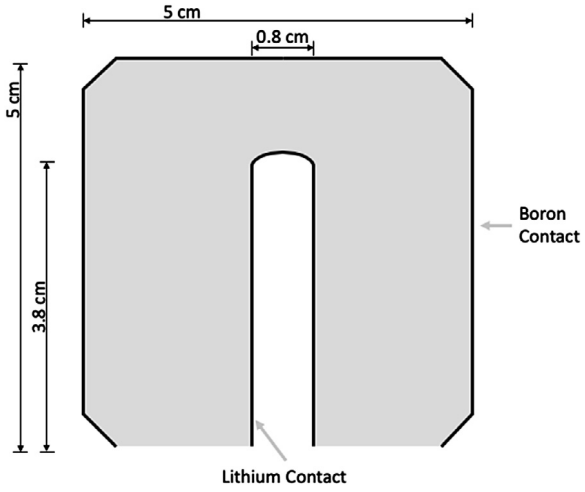

Fig. 6. Geometry of the HPGe crystal (gray) used in the Geant4 modeling, annotated to highlight the inner and outer contacts (thick black lines), whose thickness was varied as described in Section 4.4.

The absolute magnitude and slopes of the 661- and 1332-keV efficiency measurements are a close match to the expanding inner contact model (Fig. 7, right). In contrast, the expanding outer contact model indicates little difference between the two gamma-ray peak efficiencies, which sharply contrasts with our measurements. The model-to-data comparison of Fig. 7 is therefore consistent with growth of the inner (Li) contact as the cause of the loss of gamma-ray detection efficiency with anneal time.

The Li contact for our detectors was implanted within the HPGe crystal borehole via thermal diffusion, and further diffusion can occur during annealing. *Owens et al.* [15] measured a 17% loss of gamma-ray detection efficiency in n-type HPGe following 100 days (2400 h)

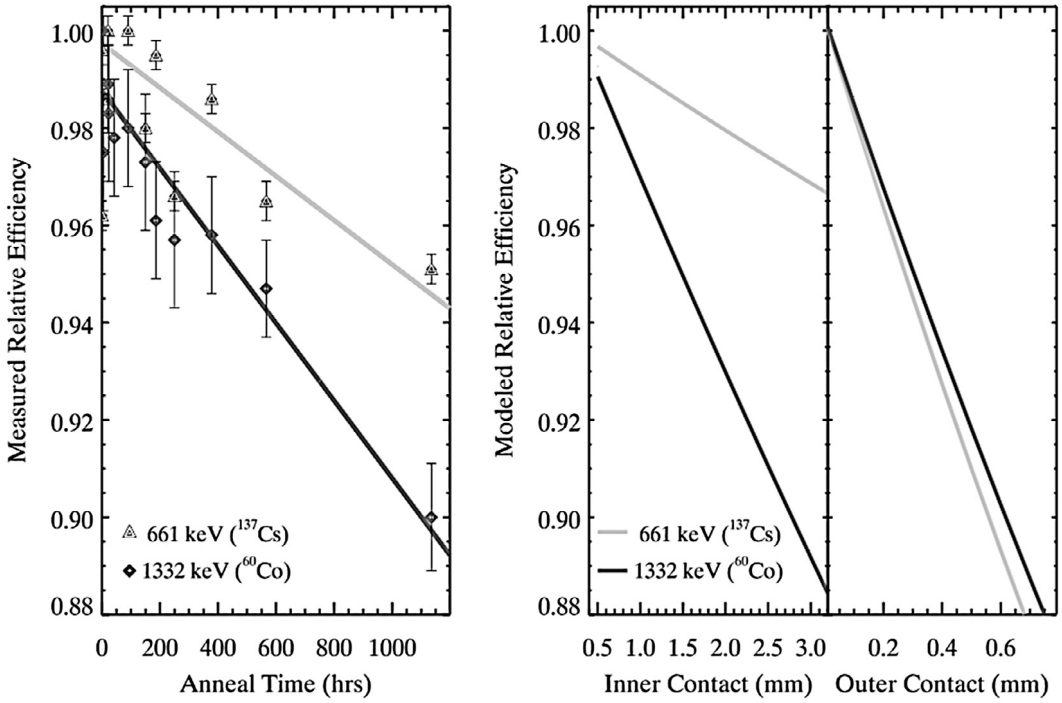

Fig. 7. (Left) Measured photopeak efficiency for detecting the 1332- and 661-keV keV gamma rays, relative to the original, pre-annealing values, plotted as a function of cumulative anneal time. (Right) Modeled photopeak detection efficiency of the 1332- and 661-keV keV gamma rays as a function of the thickness of the inner and outer contacts, relative to the original geometry.

of annealing at 100 °C, behavior they quantitatively explained using a 1-D model of Li contact growth using the Li diffusion length in Ge and Fick's diffusion laws. We repeat that calculation here for our 105 °C annealing.

Bertolini and Coche [38] report the relationship between the Li diffusion coefficient D in Ge and temperature T to be:

$$D = 2.5 \times 10^{-3} e^{-11800/RT} \quad (1)$$

in units of $cm^2\ s^{-1}$, where R is 1.98 cal K^{-1} and T is in units of K. The diffusion length L_D is then calculated as:

$$L_D = \sqrt{Dt} \quad (2)$$

in units of cm, where t is the cumulative anneal time at temperature T. *Owens et al.* assumed a linear relationship between L_D and Li contact thickness d:

$$d = nL_D, \quad (3)$$

and their data-to-model comparisons suggested $4.5 < n < 6.2$. Note that *Owens et al.* [15] and our models adopt a simplified view of the Li contact as having a sharp, well-defined boundary. In practice, the contact is a gradient with an undefined boundary. We ignore this when we adopt the *Owens et al.* n values. For those n values, and conditions of the crystal following Westinghouse anneal #8 (t = 1135 h, T = 105 °C, 378.15 K), we calculate a Li contact thickness of d = 1.7 to 2.4 mm. This value represents the increase in the lithium contact thickness (i.e. its growth) following 1135 h of annealing. Note that these equations predict growth of contacts even at room temperature, albeit slowly as compared to during annealing. This phenomenon was recently observed by [39], and may be an issue for the Psyche GRS given the mission duration (≥5 years).

Comparison of our measured and modeled efficiencies at 105 °C (Fig. 7; relative to the pre-irradiation efficiency), allows us to estimate the growth of the Li contact following the cumulative 1135 h of annealing. The measured efficiency of 90.0 ± 1.1% of the pre-irradiation efficiency (Fig. 7, left) corresponds to a modeled Li contact growth of 2.5–3.1 mm (Fig. 7, right). The range of values is due to the uncertainties of the efficiency measurement. This inferred Li contact growth (2.5–3.1 mm) is within a factor of two of the calculated d value following 1135 h of annealing (1.7–2.4 mm).

Note that the final measurements, taken after 1135 and 1371 h of annealing at 105 °C, yielded relative efficiencies of 90.0 ± 1.1% and 90.7 ± 1.0%. The consistency between these values suggests that the rate of efficiency loss decreases with increasing anneal time (Fig. 5). This is interpreted as further evidence in support of the lithium contact diffusion hypothesis, as Eqs. (1)–(3) likewise predict that the rate of change of d versus anneal time t decreases with increasing anneal time.

For spaceflight detectors, there is a desire to shorten annealing times and preserve gamma-ray detection efficiency. From an anneal duration standpoint, 115 °C is therefore preferable to 105 °C, as the time-to-recovery at these temperatures is 140 and 240 h, respectively (Fig. 3). Fits to the 105° and 115 °C data (Fig. 5) indicate that the rate of efficiency loss is higher for the 115 °C anneals (1.4% efficiency loss per 100 h) than the 105 °C anneals (0.9% efficiency loss per 100 h). We calculate that for the full-performance recovery times listed above, efficiency loss is equivalent. Thus, faster annealing does not provide a means of avoiding or limiting annealing-induced efficiency losses, although it does reduce the time needed for annealing operations.

5. Conclusions and implications for psyche GRNS and MEGANE

The GeMini Plus project produced three HPGe-based GRS systems whose design incorporated lessons learned from the MESSENGER Gamma-Ray Spectrometer. Specifically, GeMini facilitates high-temperature (up to 115 °C) annealing for full energy resolution recovery following radiation damage, and a vent-to-space design and passivated HPGe detector to avoid leakage current issues resulting from these annealing operations. These design changes were validated by a

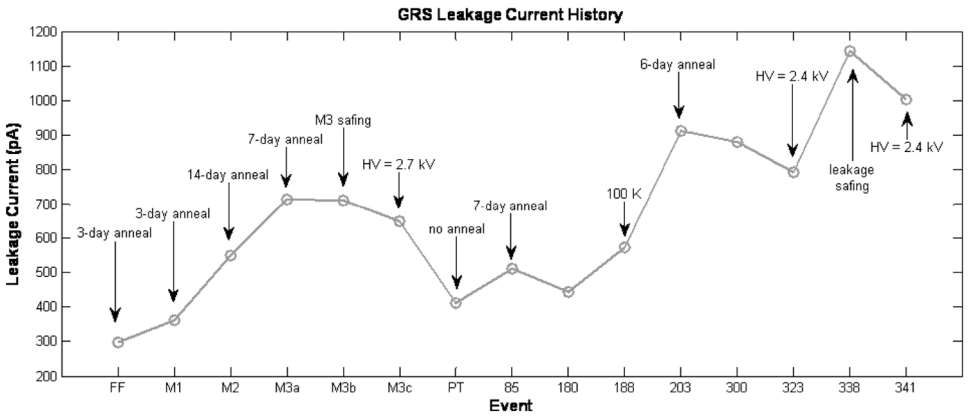

Fig. A.1. Leakage current history of the MESSENGER GRS, annotated to denote significant events in the thermal and operating history of the instrument.

campaign of detector irradiation and annealing operations. Irradiations were performed with protons having solar and galactic cosmic ray energies, and total proton fluences (Table 2) corresponding to >3 years of exposure to the interplanetary proton radiation environment. For the 1 GeV proton irradiations (8×10^8 protons cm^{-2}), annealing of the detectors at 105° and 115 °C resulted in full energy resolution recovery after 240 and 140 h of annealing, respectively. A second irradiation, 7.25×10^9 protons cm^{-2} with a solar-proton-like energy spectrum (Table 2), resulted in full recovery in <316 h of annealing at 105 °C. This irradiation mimicked the full proton environment during the 3.5-year-long interplanetary cruise to (16) Psyche, thus indicating that the Psyche GRNS (and MEGANE instruments) can expect full recovery if the systems are annealed at temperatures of ≥105 °C for a duration of at most 316 h.

MESSENGER GRS experienced increases in leakage current following each anneal (Appendix). The leakage current exceeded 1 nA following 40 days of cumulative annealing, at which point leakage current compromised the science performance of the instrument. For the GeMini systems, the initial leakage current was low (<10 pA) and there was no evidence for increased leakage currents following 57 days of cumulative annealing time on the Westinghouse detector. Thus, the vented design and passivated HPGe crystals used for the GeMini systems appears to have resolved the leakage current problems observed on MESSENGER. The Psyche GRNS and MEGANE instruments will also include a vent-to-space design and passivated HPGe crystals.

Gamma-ray photopeak detection efficiency loss was observed following annealing operations, and was determined to be strongly correlated with cumulative anneal time. The energy- and time-dependence of the efficiency loss is well-matched by radiation transport models that vary the loss of active volume at the inner borehole of the HPGe crystal, consistent with thermal diffusion of the lithium contact during annealing. These results suggest that the Psyche GRNS and MEGANE annealing strategy should be to limit anneal duration and frequency to limit efficiency loss. Inclusion of a reference gamma-ray source for in-flight monitoring of the efficiency will facilitate in-flight tracking of HPGe sensor efficiency. Without such efficiency monitoring, there is an uncharacterized systematic uncertainty associated with the efficiency of the system at its target (e.g. asteroid Psyche, Phobos) that would propagate to elemental composition measurements derived from GRS measurements.

Acknowledgments

GeMini Plus development was funded by NASAs Maturation of Instrumentation for Solar System Exploration (MatISSE) program, USA, grant NNX15AF40G. We thank Marianne Ammendolia of the Lawrence Livermore National Laboratory for providing years of technical support during the development of GeMini and GeMini Plus. We also thank Adam Rusek, Michael Sivertz, Rory Rosselot, and Jimmy Williams of the NASA Space Radiation Laboratory (NSRL) at Brookhaven National Laboratory for assistance conducting the proton irradiation experiment. Wilhelm Mueller, Mike Yocum, and Jim Colaresi of Canberra (now Mirion, Inc.) provided useful feedback as we interpreted the results of our experiments. We also thank Insoo Jun of NASA's Jet Propulsion Laboratory for providing modeled solar proton environment for the Psyche cruise, used during the second proton irradiation experiment. Finally, we thank an anonymous review for useful comments on the version of this manuscript.

Appendix. MESSENGER Lessons learned

The energy resolution of the MESSENGER GRS was 3.5 keV at launch, but gradually degraded to 5.1 keV by the time of MESSENGER's arrival at Mercury following a 6.6-year-long cruise. The energy resolution and annealing history are detailed in [7]. Incomplete energy resolution recovery was attributed to the low annealing temperature (85 °C), which prior studies have shown was insufficient to fully restore energy resolution, regardless of anneal duration [8]. MESSENGER GRS annealing also resulted in increased leakage currents, as illustrated in Fig. A.1. These increased leakage currents eventually led to degraded science performance for the instrument.

Although MESSENGER did not carry an onboard gamma-ray source, the photomultiplier tube of the GRS anti-coincidence shield was contaminated with ^{137}Cs from nuclear weapons testing fallout. This contamination provided a useful means of tracking the efficiency of the system versus time, in an attempt to identify possible efficiency loss due to thermal diffusion of the Li contact during annealing (Section 4.4). The data, shown in Fig. A.2, show a range of count rates, both above and below the expected rate due to the decay of the source alone. All pre-Orbit data are consistent (within 2 standard deviations) with the expected ^{137}Cs decay trendline, although we note that the limited ^{137}Cs decay rate and short measurements resulted in large uncertainties for these data. Once in orbit, sufficient data was available to reduce the uncertainties, and there is evidence for efficiency loss during orbital operations. The data support the need to include an onboard source with a sufficient decay rate to obtain high precision measurements of the efficiency as a function of time, particularly following annealing operations.

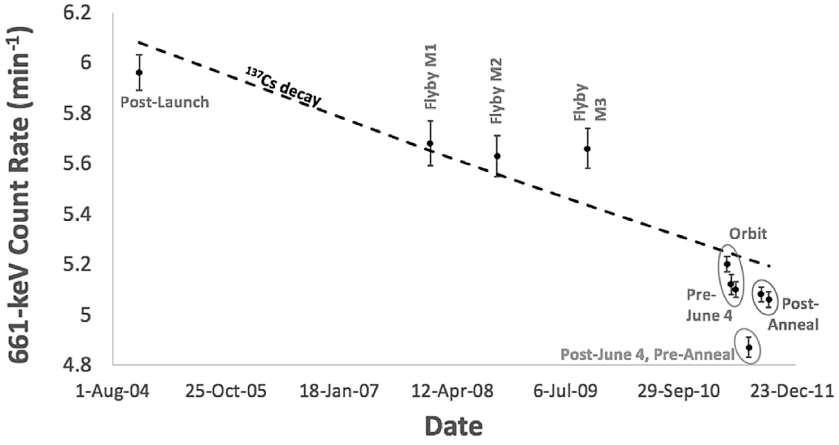

Fig. A.2. Gamma-ray photopeak efficiency at 661-keV for the MESSENGER GRS, as a function of time, with major mission events denoted. Events include the three Mercury flybys (M1, M2, M3), and post-Mercury-orbit-insertion events denoted in relation to the major SPE that occurred on June 4, 2011. This SPE degraded the energy resolution sufficiently to require an anneal. Error bars are the 1-standard-deviation errors on the 661-keV peak rate determination, and primarily result from counting statistics.

References

[1] Darken L.S., Role of disordered regions in fast-neutron damage of HPGe detectors, Nucl. Instrum. Methods Phys. Res. B 74 (4) (1993) 523–526.

[2] W.V. Boynton, W.C. Feldman, I.G. Mitrofanov, L.G. Evans, R.C. Reedy, S.W. Squyres, et al., The Mars Odyssey gamma-ray spectrometer instrument suite, Space Sci. Rev. 110 (2004) 37–83.

[3] J.O. Goldsten, E.A. Rhodes, W.V. Boynton, W.C. Feldman, D.J. Lawrence, J.I. Trombka, et al., The MESSENGER gamma-ray and neutron spectrometer, Space Sci. Rev. 131 (2007) 339–391.

[4] Hasebe Nobuyuki, et al., High performance germanium gamma-ray spectrometer on lunar polar orbiter SELENE (KAGUYA), in: Transactions of the Japan Society for Aeronautical and Space Sciences, Space Technology Japan 26, Pk_35-Pk_41.

[5] L.G. Evans, R.C. Reedy, R.D. Starr, K.E. Kerry, W.V. Boynton, Analysis of gamma ray spectra measured by Mars Odyssey, J. Geophys. Res. Planets 111 (E3) (2006).

[6] M. Kobayashi, et al., The Kaguya gamma-ray spectrometer: Instrumentation and in-flight performances, J. Instrum. 804 (2013) P04010.

[7] L.G. Evans, P.N. Peplowski, E.A. Rhodes, J.O. Goldsten, R.D. Starr, S.C. Solomon, The MESSENGER gamma-ray spectrometer: Calibration and operations, Icarus 288 (2017) 186–200.

[8] R.H. Pehl, N.W. Madden, J.H. Elliott, T.W. Raudorf, R.C. Trammell, L.S. Darken, Radiation damage resistance of reverse electrode Ge coaxial detectors, IEEE Trans. Nucl. Sci. 26 (1) (1979) 321–323.

[9] J. Bruckner, M. Korfer, H. Wanke, A.N.F. Schroeder, D. Filges, P. Dragovitsch, et al., Proton-induced radiation damage in germanium detectors, IEEE Trans. Nucl. Sci. 38 (2) (1991) 209–217.

[10] B. Kandel, V. Borrel, F. Albernhe, P. Frabel, B. Cordier, G. Tauzin, et al., Influence of temperature on the behaviour of INTEGRAL n-type HPGe detectors irradiated with fast neutrons, Nucl. Instrum. Methods Phys. Res. A 430 (2–3) (1999) 363–372.

[11] F. Albernhe, V. Borrel, P. Frabel, G. Vedrenne, R. Coszach, J.-M. Denis, P. Leleux, Degradation and recovery of Ge detectors: Tests prior to a space mission, Nucl. Instrum. Methods Phys. Res. A 492 (2002) 91–96.

[12] A. Owens, S. Brandenburg, E.J. Buis, H. Kiewiet, S. Kraft, R.W. Ostendorf, et al., An assessment of radiation damage in space-based germanium detectors due to solar proton events, Nucl. Instrum. Methods Phys. Res. A 583 (2–3) (2007) 285–301.

[13] R. Diehl, T. Siegert, J. Greiner, M. Krause, K. Kretschmer, Lang, M. Pleintinger, A.W. Strong, C. Weinberger, X. Zhang, INTEGRAL/SPI gamma-ray line spectroscopy, Astron. Astrophys. 611 (A12) (2018).

[14] J.P. Roques, S. Schanne, A. Von Kienlin, J. Knödlseder, R. Briet, L. Bouchet, et al., SPI/INTEGRAL in-flight performance, Astron. Astrophys. 411 (1) (2003) L91–L100.

[15] A. Owens, S. Brandenburg, E.J. Buis, A.G. Kozorezov, S. Kraft, R.W. Ostendorf, F. Quarati, Effect of prolonged annealing on the performance of coaxial Ge gamma-ray detectors, J. Instrum. 2 (01) (2007) P01001.

[16] D.J. Lawrence, et al., The psyche gamma-ray and neutron spectrometer: Update on instrument design and measurement capabilities, in: 50th Lunar and Planetary Science Conference, abstract 1554, 2019, https://www.hou.usra.edu/meetings/lpsc2019/pdf/1554pdf.

[17] D.J. Lawrence, et al., The Mars-moon Exploration with GAmma rays and Neutrons (MEGANE) investigation for the Martian Moon eXploration (MMX) mission, in: 49th Lunar and Planetary Science Conference, abstract 2121, 2018, https://www.hou.usra.edu/meetings/lpsc2018/pdf/2121pdf.

[18] M.T. Burks, L.E. Heffern, D.J. Lawrence, J.O. Goldsten, P.N. Peplowski, GeMini Plus: A versatile gamma-ray spectrometer for planetary science composition measurements, in: 3rd International Workshop on Instrumentation for Planetary Science Missions, abstract 4087, 2016, https://www.hou.usra.edu/meetings/ipm2016/pdf/4087pdf.

[19] M.T. Burks, O.B. Drury, J.O. Goldsten, D.J. Lawrence, P.N. Peplowski, Z.W. Yokley, Emerging role of high-purity germanium detector for planetary science, in: 49th Lunar and Planetary Science Conference, abstract 1802, 2018, https://www.hou.usra.edu/meetings/lpsc2018/pdf/1802pdf.

[20] Knoll G.F., Radiation and Detection, second ed., John Wiley and Sons, Inc, Hoboken, NJ, 1999.

[21] Hull E. L., Charge Collection Physics in Germanium Detectors (Thesis), Department of Physics, Indiana University, 1998.

[22] P.N. Peplowski, L.G. Evans, S.A. Hauck, T.J. McCoy, W.V. Boynton, J.J. Gillis-Davis, et al., Radioactive elements on Mercury's surface from MESSENGER: Implications for the planet's formation and evolution, Science 333 (6051) (2011) 1850–1852.

[23] M. Koenen, J. Bruckner, M. Korfer, I. Taylor, H. Wanke, Radiation damage in large-volume n-and p-type high-purity germanium detectors irradiated by 1.5 GeV protons, IEEE Trans. Nucl. Sci. 42 (4) (1995) 653–658.

[24] R.H. Pehl, P.N. Luke, D.L. Friesel, High-purity germanium charged-particle detectors: A LBL-IUCF update, Nucl. Instrum. Methods Phys. Res. A 242 (1) (1985) 103–110.

[25] V. Borrel, B. Kandel, F. Albernhe, P. Frabel, B. Cordier, G. Tauzin, et al., Fast neutron-induced damage in INTEGRAL n-type HPGe detectors, Nucl. Instrum. Methods Phys. Res. A 430 (2–3) (1999) 348–362.

[26] J.A. Simpson, Elemental and isotopic composition of the galactic cosmic rays, Annu. Rev. Nuclear Part. Sci. 33.1 (1983) 323–382.

[27] O. Adriani, G.C. Barbarino, G.A. Bazilevskaya, R. Bellotti, M. Boezio, E.A. Bogomolov, L. Bonechi, et al., PAMELA measurements of cosmic-ray proton and helium spectra, Science 332 (6025) (2011) 69–72.

[28] J. Feynman, A. Ruzmaikin, Berdichevsky V., The JPL proton fluence model: An update, J. Atmos. Sol.-Terr. Phys. 64 (2002) 1679–1686.

[29] B. Pirard, J. Cabrera, C. d'Uston, J.J. Thocaven, O. Gasnault, P. Leleux, J. Brückner, Solar proton damage in high-purity germanium detectors, Nucl. Instrum. Methods Phys. Res. A 572 (2) (2007) 698–707.

[30] G. Castagnoli, D. Lal, Solar modulation effects in terrestrial production of carbon-14, Radiocarbon 22 (2) (1980) 133–158.

[31] D. Lal, Theoretically expected variations in the terrestrial cosmic-ray production rates of isotopes, in: G.C. Castagnoli (Ed.), Solar-Terrestrial Relationships and the Earth Environment in the Last Millenia, Proc. Internat. School Phys. Enrico Fermi 95 (1985) 216–233.

[32] P.N. Peplowski, J.T. Wilson, M. Burks, A.W. Beck, I. Jun, D.J. Lawrence, Z.W. Yokley, Cosmogenic radionuclide production modeling with Geant4: Experimental benchmarking and application to nuclear spectroscopy of asteroid (16) Psyche, Nucl. Instrum. Methods Phys. Res. B 446 (2019) 43–57.

[33] A. Owens, R. Baker, T.L. Cline, N. Gehrels, J. Jermakian, T. Nolan, et al., The transient gamma-ray spectrometer, IEEE Trans. Nucl. Sci. 38 (2) (1991) 559–567.

[34] D.I. Lowenstein, A. Rusek, Technical developments at the NASA space radiation laboratory, Radiat. Environ. Biophys. 46 (2007) 91–94.

[35] N. Tsoupas, L. Ahrens, S. Bellavia, R. Bonati, K.A. Brown, I-Hung Chiang, C.J. Gardener, D. Gassner, S. Jao, W.W. Mackay, I. Marneris, W. Meng, D. Phillips, P. Pile, R. Prigl, A. Rusek, L. Syndstrup, K. Zeno, Uniform beam distributions at the target of the NASA space radiation laboratory's beam line, Phys. Rev. ST Accel. Beams 10 (2007) 024701.

[36] C. La Tessa, M. Sivertz, I.-H. Chiang, D. Lowenstein, A. Rusek, Overview of the NASA space radiation laboratory, Life Sci. Space Res. 11 (2016) 18–23.
[37] E.L. Hull, R.H. Pehl, N.W. Madden, P.N. Luke, C.P. Cork, D.L. Malone, et al., Temperature sensitivity of surface channel effects on high-purity germanium detectors, Nucl. Instrum. Methods Phys. Res. A 364 (3) (1995) 488–495.
[38] G. Bertolini, A. Coche, Semiconductor Detectors, North Holland Publishing Co, New York City, 1968.
[39] E.R. van der Graaf, P. Dendooven, S. Brandenburg, Using standard calibrated geometries to characterize a coaxial high purity germanium gamma detector for Monte Carlo simulations, Rev. Sci. Instrum. 85.6 (2014) 065110.